

Prototype study of the Cherenkov imager of the AMS experiment

P. Aguayo^a, M. Aguilar-Benitez^a, L. Arruda^b, F. Barao^b, G. Barreira^b, A. Barrau^c, B. Baret^c, E. Belmont^d, J. Berdugo^a, G. Boudoul^c, J. Borges^b, M. Buénerd^{c,*}, D. Casadei^c, J. Casaus^a, C. Delgado^a, C. Diaz^a, L. Derome^c, L. Eraud^c, L. Gallin-Martel^c, F. Giovacchini^c, P. Goncalves^b, E. Lanciotti^a, G. Laurenti^c, A. Malinine^f, C. Mañá^a, J. Marín^a, G. Martinez^a, A. Menchaca-Rocha^d, C. Palomares^a, R. Pereira^b, M. Pimenta^b, K. Protasov^c, E. Sanchez^a, E.-S. Seo^f, I. Sevilla^a, A. Torrentó^a, M. Vargas-Trevino^c, O. Véziat^c

^aCIEMAT, Avenida Complutense 22, E-28040 Madrid, Spain

^bLIP, Avenida Elias Garcia 14-1, P-1000 Lisboa, Portugal

^cLPSC, IN2P3/CNRS, 53 av. des Martyrs, 38026 Grenoble cedex, France

^dInstituto de Fisica, UNAM, AP 20-364 Mexico DF, Mexico

^eUniversity of Bologna and INFN, Via Irnerio 46, I-40126 Bologna, Italy

^fUniversity of Maryland, College Park, MD 20742, USA

Received 3 October 2005; accepted 4 January 2006

Available online 31 January 2006

Abstract

The AMS experiment includes a Cherenkov imager for mass and charge identification of charged cosmic rays. A second generation prototype has been constructed and its performances evaluated both with cosmic ray particles and with beam ions. In-beam tests have been performed using secondary nuclei from the fragmentation of 20 GeV/c per nucleon Pb ions and 158 GeV/c per nucleon In from the CERN SPS in 2002 and 2003. Partial results are reported. The performances of the prototype for the velocity and the charge measurements have been studied over the range of ion charge $Z \lesssim 30$. A sample of candidate silica aerogel radiators for the flight model of the detector has been tested. The measured velocity resolution of the detector was found to scale with Z^{-1} as expected, with a value $\sigma(\beta)/\beta \approx 0.7\text{--}110^{-3}$ for singly charged particles and an asymptotic limit in Z of $0.4\text{--}0.6 \times 10^{-4}$. The measured charge resolution obtained for the $n = 1.05$ aerogel radiator material selected for the flight model of the detector is $\sigma(Z) = 0.18$ (statistical) \oplus 0.015 (systematic), ensuring a good charge separation up to the iron element, for the prototype in the reported experimental conditions.

© 2006 Elsevier B.V. All rights reserved.

PACS: 07.87.+v; 07.77.Ka; 29.40.Ka

Keywords: Space instrumentation; Cherenkov imaging; Charged particle detectors; Charge measurement

1. Introduction

The AMS spectrometer stands at the forefront of the new generation of instruments for space experiments. It is a large acceptance ($0.5\text{m}^2\text{sr}$) detector based on a superconducting magnet designed for long-duration operation in space. It will be installed on the International Space Station (ISS) for a long-term experimental campaign of three or

more years. The main purposes of the experiment are the search for primordial antimatter and for dark matter in space [1]. In addition, the instrumental capabilities of the experiment for momentum measurement and particle identification required for these studies also open highly promising prospects for other astrophysics and astroparticle physics studies involving cosmic ray (CR) detection, from γ to nuclear particles. The ion mass and charge identification capabilities obtained by means of the Cherenkov imager will make possible a high statistics study of the composition and of the momentum spectrum

*Corresponding author. Tel.: +33 476 284 082; fax: +33 476 284 004.

E-mail address: buenerd@lpsc.in2p3.fr (M. Buénerd).

of the cosmic ray flux over a mass-charge-momentum range, unmatched so far in a single space experiment. The instrumental architecture of the AMS spectrometer is described elsewhere [1,2].

In the variety of the possible optical solutions for the Cherenkov imager, the proximity focusing technique [3] appeared to be the most suitable since the instrument has to cover a large geometrical acceptance with a basically isotropic particle flux to be studied. The momentum range to be covered implied the use of a low refractive index solid state Cherenkov radiator, a requirement conveniently matched by the silica aerogel material recently developed and commonly used today in particle physics experiments since the pioneering work of Ref. [4].

The basic configuration of the instrument has been discussed in detail in a previous prototype study [5] and in a preliminary simulation work [6]. These studies have shown that the counter can be expected to provide a measurement of the charged particles velocity with a precision of the order of $\sigma(\beta)/\beta \simeq 10^{-3}$ for $\beta = 1$ and $Z = 1$ particles, for the considered configuration. In such a counter, the velocity resolution is limited by contributions from the radiator thickness, radiator material chromatism, and from the spatial resolution of the detector (pixel size for pixelized detector). The combination of the velocity measured by the RICH with the momentum measured by the tracker ($\Delta P/P \simeq 2\%$ over the relevant momentum range for $Z = 1$ particles) will provide a determination of the particle mass extending expectedly from ~ 1 GeV/nucleon up to around ~ 10 GeV/nucleon kinetic energy, for the low range of nuclear masses. The momentum coverage for mass ID will be obtained by combining two radiators: sodium fluoride between 1 and 5 GeV/c per nucleon, and silica aerogel ($n \approx 1.03$ – 1.05) for higher momenta with a comfortable overlap for intermediate momentum values. In addition, for each event, the measurement of the Cherenkov light yield by photon counting should provide a measurement of the charge of the particles with a good single element separation, i.e., with a resolution better than 0.3 charge unit, up to around $Z \simeq 26$ (Fe). These performances are suitably matching the requirements of the physics program for CR study, and they open a broad research field for CRs in AMS. In particular, the whole momentum range is of major physical interest for the flux measurement of the long life ^{10}Be isotope, our best available galactic clock [9,10]. This is true as well for the CR secondary over primary flux ratio over the considered range of elements.

A new prototype of the counter has been built to investigate the expected performances and to validate the techniques used and the instrumental options taken, for a design close to the flight model. This paper reports on the experimental study of this prototype. Its performances have been investigated for different radiators both with CR particles and with a 20 and 158 GeV/c per nucleon beams of secondary ions at the CERN SPS facility. These beams were developed to this purpose, to provide simultaneously

nuclei with $1 \leq Z \leq 45$ through the counter [7]. These latter results constitute the bulk of the report. Another major purpose of the study was to select the flight model Cherenkov radiator.

The measurement results with the prototype operated with a sodium fluoride radiator and with a prototype of the RICH conical mirror will be presented in a forthcoming publication.

The paper is organized as follows. The AMS RICH project is briefly outlined in the next section. Section 3 reports on the presentation and on the general features of the prototype, on the photomultiplier (PMT) calibration and linearity study. Section 4 reports on the beam tests, beam development and experimental setup. The measurements performed are described in Section 5 and their results are discussed in Section 6. The work is summarized and concluded in Section 7.

2. The AMS RICH counter

The imager was described previously in Ref. [8]. The design has to meet a set of specific constraints imposed by the launch and flight conditions, on the resistance to vibrations of the structure and of its elements, and on the volume and shape of the payload, as well as by the particular experimental environment of a long duration spatial experiment. The latter bear in particular on the weight, power consumption of the apparatus, and long-term reliability of components. In addition, another very specific operating condition in AMS is due to the ambient (stray) magnetic field induced by the neighbouring superconducting magnet over the photon detector volume, reaching about 300 G in some regions of the counter. The functional architecture consists of a radiator plane placed at the top of the counter, separated from the photon detector plane at the bottom of the counter, by a photon drift space, or ring expansion gap, ~ 46 cm deep. The detector plane has an empty $64 \times 64 \text{ cm}^2$ area in its centre, matching the active area of the electromagnetic calorimeter (ECAL) located below. These elements are enclosed in the volume of a conical mirror, the purpose of the latter being of maximizing the geometrical acceptance. The radiator plane is a dodecahedral polygon with a 118.5 cm internal tangent diameter. It consists of an array of aerogel tiles with a refractive index with $n = 1.03$ – 1.05 , 2.7 cm thick surrounding a the central $\approx 35 \times 35 \text{ cm}^2$ region equipped with 5 mm thick sodium fluoride (NaF, $n \approx 1.33$) radiator. This radiator combination optimizes the overall counter acceptance, since the Cherenkov photons radiated by the NaF will fall within the detector area, while photons radiated by aerogel from the same location would fall in the ECAL hole [11]. Outside the ECAL hole, 680 4×4 -multianode PMTs are arranged to cover the circular 134 cm diameter surface at the basis of the conical mirror.

3. The RICH prototype

The prototype has been described previously in Ref. [8]. It consists of an array of 9×11 cells corresponding to about 14% of the total number of channels of the AMS RICH. It has a $31 \times 31 \text{ mm}^2$ total optical surface and is equipped with a 4×4 pixels $4.5 \times 4.5 \text{ mm}^2$ each, multi-anode Hamamatsu R7600-M16 photomultiplier [13]. In each cell, the light collection is achieved by means of a matrix of 4×4 light guides, matching the pixel pattern of the PMT, with an effective pixel surface of $7.55 \times 7.55 \text{ mm}^2$, the pixel coordinates providing the photon hit position. Inside the AMS spectrometer, the PMTs will have to be efficiently shielded against the stray magnetic field of the superconducting magnet (up to $\sim 300 \text{ G}$) [2]. To reach the required efficiency, the (individual) shieldings have to extend by about 30 mm beyond the entrance window of the tubes. Each cell then consists of a PMT, lightguide array, HV divider plus front-end (FE) electronics, all housed and potted in a plastic shell and then enclosed in a magnetic shielding.

The mechanical arrangement reproduces the flight model configuration to make the present validation tests significant. The different radiators studied were placed at adjustable distance from the detector plane by means of a mechanical support. The expansion gaps used during the tests were set in order to have fully contained events on the detection matrix, while being comparable to the flight design.

The flight model version of the FE electronics [14] was used throughout this study. The data acquisition electronics (DAQ) was based on the general purpose DAQ designed for the needs of the AMS subdetectors development and construction [15,16].

Fig. 1 shows a photographic view of the prototype setup.

3.1. PMT calibration

An accurate PMT calibration is a key condition to reach the best possible counter resolution for the particle charge measurements [6]. It is also necessary because the PMTs are powered by groups of 9 or 10 units with the same HV regulators, which requires the tubes to be sorted by gains so that any groups controlled by a given HV unit have their gains contained in a narrow range, with the purpose of maximizing the dynamic range. This arrangement provides a uniform response of the photodetection matrix and the gain spread inside the groups does not limit the dynamical range of operation of the counter. A first LED calibration of the tubes was performed in the laboratory by means of a dedicated test bench. The PMTs were thus arranged in the prototype according to their measured gains. In Fig. 2 the response of a PMT illuminated in the single photoelectron regime is shown. The fitted function corresponds to a sum of a Gaussian shape modelling the pedestal and a set of n -photoelectron response functions, whose respective amplitudes are constrained by the Poisson distribution envelope

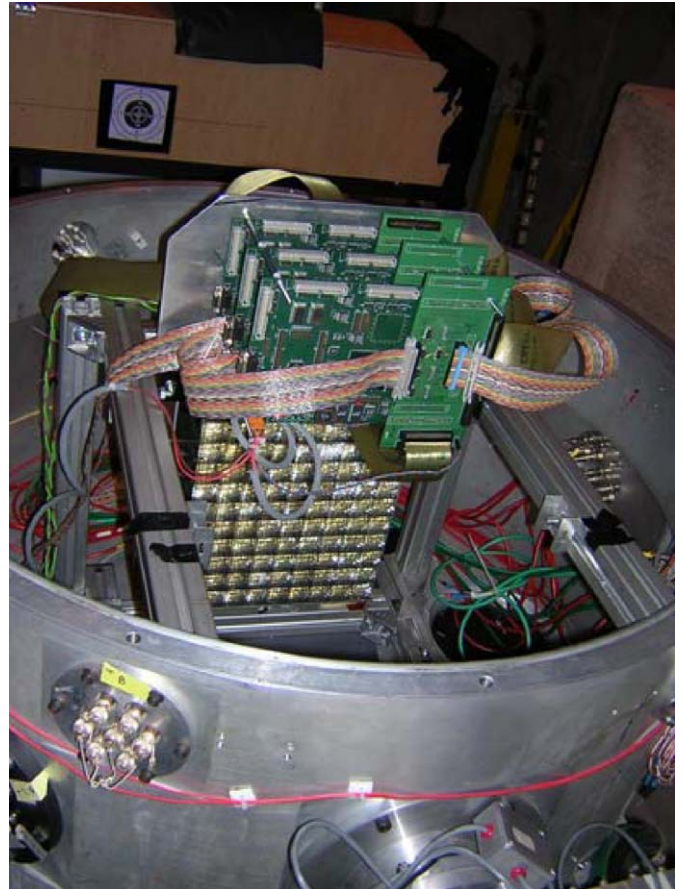


Fig. 1. Photographic view of the prototype setup during the beam tests at CERN.

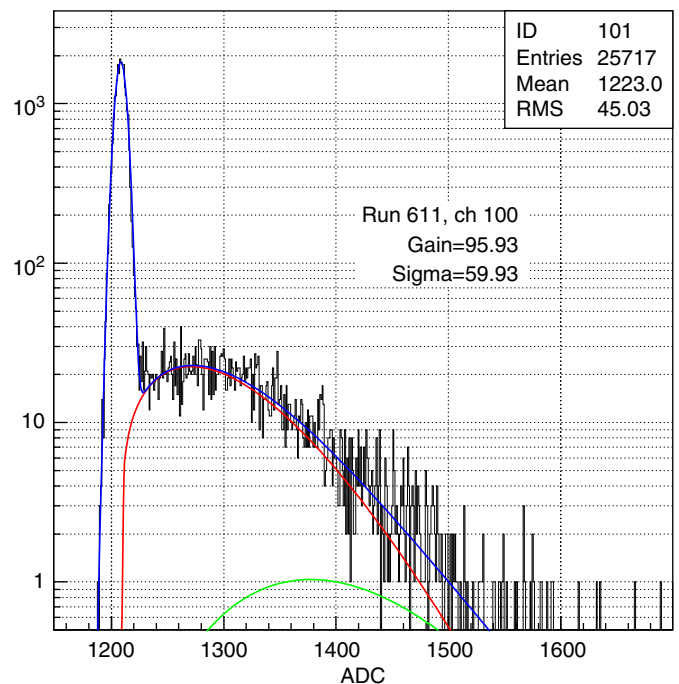


Fig. 2. Spectrum of the PMT response in single photoelectron regime, fitted with the set of functions as described in the text.

of the statistical weights. The PMT response to single photoelectron is parametrized with a biparametric function to estimate its gain and single photoelectron resolution [30]. During the test beam periods, specific calibration LED runs were taken for the purpose of PMT gain monitoring. In these data, the single pixel response was fitted using the same functional form as described above. In addition to the LED runs, global drifts of the gains were continuously monitored in the normal data taking runs through the single channel average response. The average gain relative to a reference value is shown in Fig. 3. Variations smaller than 1% are observed within a single run. Moreover, the evaluation of this latter quantity during the full data taking period shows a stability of the average response within a 2% variation level, which is consistent with the determination from the LED calibration runs.

3.1.1. Linearity measurements

The PMT linearity was measured using a set of accurately calibrated optical filters [17]. A reference signal of about 10 photoelectrons was chosen. This value was large enough to ensure the amplitude distribution of the corresponding detected signal to be already Gaussian and it was small enough to ensure this response to be still in the linear region. The filters were then removed by steps and the increase of the measured signal could be compared with the increase of the (so calibrated) incident light. Fig. 4 shows the results obtained. Some non-linearity was induced, however, for large amplitude signals by a minor change in the HV divider, in the 2002 run data. It was corrected in the analysis by using an effective non-linear saturation-like response of the tubes.

The linearity characteristics do not depend on the high-voltage divider (HVD) associated to the PMT. Customary (6.6 MΩ total resistance) and a very low current (80 MΩ) HVDs have been tested. The HV repartition used was 2.4-2.4-1-1-1-1-1-1-1-1-1.2-2.4-2.4, as recommended by the manufacturer [19], in both cases. The 80 MΩ HVD is the type to be used in the flight model since power consumption is critically limited in the payload, and since the

expected rather low count rate in AMS allows such an option to be used.

4. Tests of the imager prototype

The counter has been first studied with CR (mostly muon) particles, on the ground. The same instrumental environment (vacuum chamber, tracker, trigger detectors and electronics, DAQ computer and software) was used for this step as for the study prototype [5]. The measurements allowed to obtain estimates of the velocity and charge resolutions of the device and to test material radiators [18,8,20]. However, cosmic muons suffer some significant limitations: the velocity resolution cannot be measured

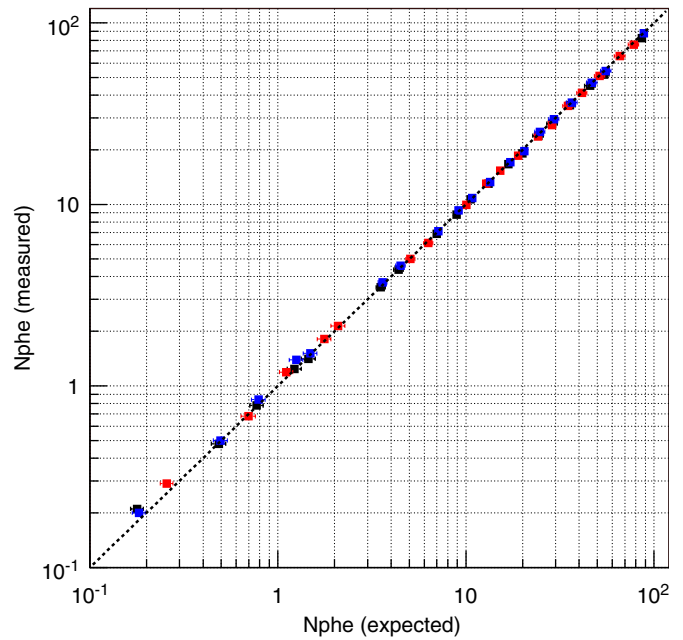


Fig. 4. Linearity measurements results obtained as described in the text, for the PMTs used in the prototype, for two different sockets with total resistance for the high voltage dividers of 6.6 and 80 MΩ, respectively, corresponding to the standard manufacturer-recommended HV divider, and the flight model divider, respectively.

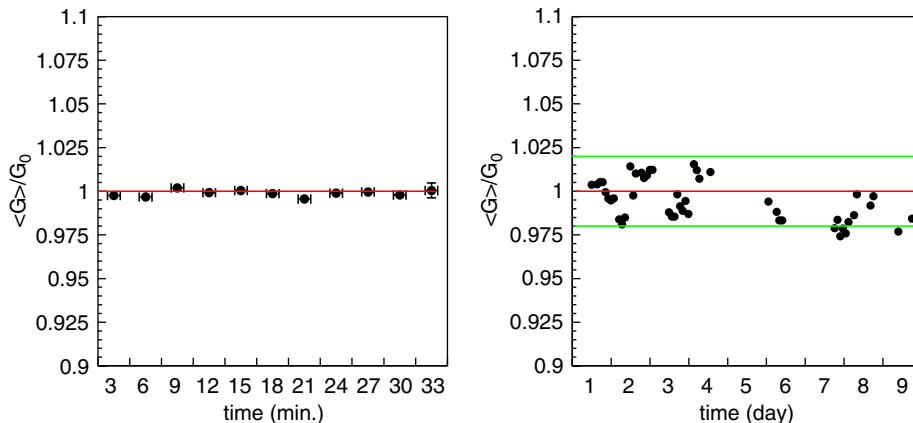


Fig. 3. Evolution of the mean gain per channel relative to its reference value, G_0 , along a single run (left) and along the whole period of data taking (right).

accurately since the particle momentum cannot be easily measured to the required accuracy. Since the main purpose of the RICH is isotope identification, i.e. nuclear particles charge and mass measurement, it was important to study the response of the counter through its nominal range of Z values. Some in-beam tests with a suitable control of the particle momentum and of the beam intensity were thus highly wishable for a good calibration of the apparatus and a good knowledge of its response to ions.

The in-beam experimentation of the apparatus has allowed to achieve an end-to-end testing of the instrument with an ion distribution similar to the CR flux in space. The physics basis of the beam design and the main beam features are described in Ref. [7]. The principle is recalled here briefly for the reader's convenience. The secondary ion beam was produced by fragmentation of a primary ion beam on a production target located just after the extraction channel of the SPS. Downstream from this target, the secondary products were filtered by magnetic analysis in the beam transport line, and the rigidity setting of the line allowed the nuclear fragments to be selected according to their mass over charge ratio A/Z .

The secondary beams were obtained by bombardment of a Be production target with 10^7 20 GeV/ c /nucleon Pb ions per spill from the CERN SPS in the 2002 run, while in 2003, a 158 GeV/ c /nucleon Indium beam onto a Pb target was used, with a similar intensity. For the $A/Z = 2$ beam setting, the envelope of the charge distribution of the nuclear elements with $Z \lesssim 26$ in the beam turned out to be similar enough to the experimental abundance distribution of CRs to make such beams useful substitutes on the ground of the nuclear CR flux in space.

4.1. Ion beam line and optics

The H8 beam line at CERN has a momentum resolution $0.15\% \leq \Delta P/P \leq 1.5\%$. This was particularly convenient for the purpose of the test, since the beam momentum resolution could be set to the same value as expected for the AMS magnetic spectrometer [21]. The optics of the line was tuned so as to provide a beam as close to parallel as possible, with a divergence of the order of 1–2 mrad. The resulting beam profile was conveniently broad with a width on the scale of 5 mm in 2002 setting, whereas it was much narrower in 2003, with a section of 2–3 mm. The beam intensities used were in the range 10^2 – 10^3 particles per spill. In the 2003 run the beam was more focussed and the beam divergence was less than 1 mrad.

The beam content in nuclear elements could be selected according to the desired A/Z value of the fragmentation products transported in the beam line, by tuning the beam line rigidity setting to the appropriate value. Three main settings were used: $A/Z = 2$ for inclusive mass range, $A/Z = \frac{3}{2}$ to enhance the ^3He intensity, and $A/Z = \frac{7}{4}$ for ^7Be enhancement. Single charge particles with momenta between 5 and 13 GeV/ c were also used for dedicated measurements.

4.2. Experimental setup

The configurations used for the in-beam tests were about the same as used previously for the study prototype [5], with some minor changes. Two plastic scintillators provided the DAQ trigger while one or two multiwire proportional chamber(s) (xy) were used for simple tracking and determination of the beam particle hit position on the detector. In the 2003 run the information from a prototype of the AMS tracker [21] placed upstream was incorporated to the data flow.

The prototype was placed inside a light-tight container. Two trigger scintillators were placed about 1 m apart in front of the container to provide the trigger coincidence. A delay line readout multiwire proportional chamber (MWPC), with 2.5 mm pitch horizontal anode wires and 0.7 mm pitch vertical strips on the influence plane, was placed in front of the upstream trigger scintillator. It provided the transverse coordinates of the particle trajectory with a typical fraction of mm accuracy, good enough to help on the event definition in the 2002 run.

In 2003, the presence of the silicon tracker prototype on the same beam line provided a very precise measurement of the particle track parameters for the event reconstruction. The difference in the experimental setups together with the different beam size and divergence leads to minor variations in the event selection and analysis algorithms between the two runs.

A representative subset of the studied radiators is listed in Table 1. They consisted of 11, 25 and 30 mm thick tiles of silica aerogel with different refractive index (n). The 11 mm tiles were stacked in groups of two or three to get the desired radiator thickness (d). They were placed at variable distances (photon drift gap, h) from the detection plane. The sample was provided by two manufacturers: Matsushita Electric Co. [22] (11 mm thick tiles of hydrophobic material, referred to as MEC in the following), and

Table 1

Silica aerogels studied in this work, with drift gap h used for the tests, thickness d of the samples, and number of tiles in the stack

Manufacturer	n	h (mm)	Thickness (mm)
<i>2002 run</i>			
MECy01.103	1.03	422.5	3×11
MECy02.103	1.03	422.5	2×11
MECy02.105	1.05	375.0	2×11
CINy02.103	1.03	422.5	30
<i>2003 run</i>			
MECy03.103	1.03	334,423	3×11
CINy02.103	1.03	334,423	30
CINy03.105	1.05	334,353	25

The nomenclature used is defined as XORyDAT.IND, where XOR stands for the origin of the product (MEC or CIN), DAT indicates the approximate production year, and IND refers to the nominal value of the refraction index. For example, MECy01.103 means a MEC tile with index 1.03 produced in 2001. The same convention is used throughout the paper.

Catalysis Institute of Novosibirsk [23] (25 and 30 mm thick tiles of hydrophilic, referred to as CIN). It is important to note that the same tile of radiator, the sample of CINy02.103, was used in both runs. The comparison of the results relative to this radiator has allowed to prove the setup stability and the aerogel performance after one year period.

5. Measurements and results

The reported measurements were performed in two runs in October 2002 and October 2003. About 5 million events were recorded in the first (4 days) run on a representative sample of radiators, while about 11 million events were recorded from the second run (7 days) in similar experimental conditions. Fig. 5 shows a few examples of Cherenkov rings measured for various ions through the covered range of charge with the $A/Z = 2$ setting of the beam line rigidity.

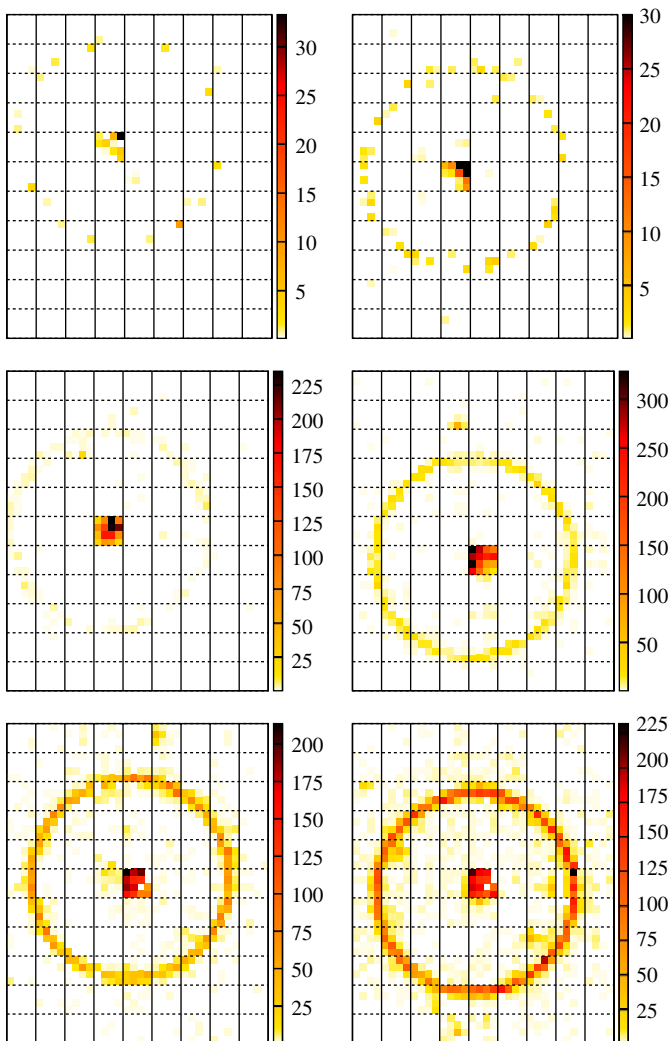


Fig. 5. Examples of Cherenkov rings measured with the beam of ion fragments. The patterns correspond to $Z = 2, 3, 6, 16, 26,$ and about 40 , from left to right and from top to bottom.

5.1. Front-end electronics

One of the primary goals of the test was to investigate the response of the FE electronics to particles over the nominal range of mass and charge of the counter. From this point of view, the tests have been extremely instructive and useful, allowing significant corrections and improvements of the readout electronics control sequence to be achieved [14]. The stability of the FE electronics was also tested on the time scale of the run duration, i.e. a week. It appeared out to be good enough not to alter the measurement accuracy.

5.2. Velocity and charge reconstruction

The velocity (β) and the absolute value of the electric charge of the ions (Z) were determined using the reconstruction algorithms developed for the final counter and adapted to the prototype. For this particular setup, the transverse coordinates (x, y) of the particle's trajectory measured by the MWPC (for the 2002 run) or by the tracker prototype (for most of the data of 2003) were used. For the latter, the measurement of the particle direction provided by the tracker was included as an input in the reconstruction. For 2002 runs, since no measurement of the particle direction was available, the ring reconstruction procedure started with the trial assumption of a track perpendicular to the detection plane, therefore neglecting the beam divergence, and the particle direction was estimated from the reconstructed ring.

Two different approaches were implemented for the Cherenkov ring reconstruction. One was based on single hit reconstruction [18], and the other on a maximum likelihood method [24]. In the former method a value of β is reconstructed for each detected hit. Next, the most probable cluster of hits is searched, and the final velocity is computed as a mean of the β value of the hits from the cluster, weighted with the measured signal amplitude (photon multiplicity). In the other reconstruction approach, the algorithm incorporates the probability density function for the signal hits, Gaussian distributed around the true Cherenkov angle, and the background hits, which have a flat distribution. The results obtained with both methods are compatible.

The reconstructed charge is determined using the estimator $Z_{\text{meas}} = \sqrt{N_{\text{ring}}/N_{\text{exp}}}$ where N_{ring} is the number of photoelectrons detected in the ring and N_{exp} is the number of expected p.e. for an equivalent (same velocity and same track parameters) $Z = 1$ particle [12]. The computation of N_{exp} is done on an event by event basis using either semi-analytical or numerical methods to account for the detector geometrical acceptance, the transmittance of the optical elements in the system and the photodetection plane efficiency. A high accuracy in this computation is necessary to keep the charge confusion at level of 1% for the flight setup, where the acceptance of the

detector is nonhomogeneous mainly due to the ECAL gap in the detection plane.

5.3. Event selection

The event selection was mainly intended to remove wrongly reconstructed tracks and to reject multiparticle events dominantly arising either from fragmented beam particles or due to δ -ray emission. First, consistency between the external determination of the track transverse coordinates and the estimation from the reconstructed ring is required. Then, events with more than one particle hit in the PMT plane are rejected. Furthermore, in order to avoid spurious contributions to the estimated velocity resolution, only events associated to tracks with small (<1.3 mrad) divergence are selected. A more extensive study of the event selection can be found in Ref. [18].

5.4. Photon yield

The light yield has been derived from the analysis of helium samples collected with the $A/Z = 2$ setting of the beam line and confirmed with an independent evaluation from proton data samples gathered during the test beam of October 2002. The reconstructed Cherenkov light yield for the different samples is shown in Table 2, where N_{exp} is the number of p.e. in the ring for particles of $\beta \sim 1$ and $Z = 1$ and fully contained events. The systematic error reported in the table has been estimated directly from data, as will be described in Section 5.5. The values of N_{exp} from the different samples are significantly widespread, varying from about 6 p.e. for the MECy02.103 sample to about 15 p.e. for CINy03.105.

Radiators with high index are expected to have a larger photon yield. It is the case for the CINy03.105 tile (~ 15 p.e.), which provides the largest photon multiplicity of the studied set, while the slightly thinner MECy02.105 tile with the same index shows a significantly lower photon yield, indicating poorer optical transmission properties. Among the low index radiators (i.e. 1.03), the oldest Matsushita

batches (MECy01.103 and MECy02.103) provide the lowest p.e. multiplicity (8 and 6 p.e., respectively) while the recent 2003 sample (MECy03.103) is noticeably better (~ 11 p.e.). The CINy02.103 Novosibirsk sample has a good photon yield (~ 10.5 p.e.), close to that of MECy03.103. Note that the comparison is somewhat qualitative since the different samples have also different thicknesses.

The analysis of the proton data samples collected at different energies during the 2002 test beam period provided an independent determination of the photon yield of the available radiators at that time. Fig. 6 (left) shows the reconstructed mean light yield variation as a function of the proton beam momentum for fully contained rings. The Cherenkov ring acceptance variation, caused by the large beam spread, was taken into account in the evaluation procedure. To compensate the lost signal due to the DAQ lower threshold, an additional correction of the order of 5–10% was estimated and applied to the detected number of photoelectrons. In order to derive the number of photoelectrons N_0 for $\beta = 1$, the data were fitted with the expected momentum dependence $N = N_0(1 - (m^2/p^2(n^2 - 1)))$, where m is the proton mass and n the refractive index. The values obtained from the fits are consistent with the photon yield determination from helium samples. The light yield, corrected for its momentum dependence, is shown in Fig. 6 (right). The quality of the agreement of the data with the theoretical curve is a clear indication of a uniform efficiency of the detector plane for incident angles ranging up to around 20° .

The photon yield of the radiator CINy02.103 in 2003 run shows an increase of about 6% with respect to the 2002 data. The main contribution to this discrepancy is likely due to the higher gains at which the PMTs were operating in 2003 (a factor 2 of higher than in 2002) and/or to the optimized settings of the FE electronics timing (peaking times sampling for the measured amplitudes), which resulted in a rise of the average PMT gain from ~ 60 ADC counts in the 2002 setup up to ~ 120 ADC counts for the spe, in 2003, making more efficient the detection of low charge hits. This comparison discards any sizeable long-term deterioration of the system.

5.5. Charge measurement

Examples of reconstructed charge distributions obtained as described in Section 5.2 are shown in Fig. 7. The two spectra display a structure of well separated individual peaks over the whole range of charge, up to $Z = 26$ (Fe), each peak expectedly corresponding to a single element. Note that the very low $Z = 4$ yield in Fig. 7 is due to the absence of the (unbound) ^8Be isotope in the $A/Z = 2$ beam. The peak is only populated by the small admixture of $^{7,9}\text{Be}$ neighbouring isotopes transported by the beam line for this rigidity setting. This was confirmed by the observed correlations between the reconstructed Z spectrum and the dE/dx spectrum of the trigger scintillators.

Table 2
Photon yield for all the sample of aerogel analysed

Manufacturer	Thickness (mm)	$N_{\text{exp}} \pm \Delta_{\text{sys}}$ (p.e.)
<i>2002 run</i>		
MECy01.103	3 × 11	8.23 ± 0.16
MECy02.103	2 × 11	5.88 ± 0.12
MECy02.105	2 × 11	9.29 ± 0.18
CINy02.103	30	9.78 ± 0.15
<i>2003 run</i>		
MECy03.103	3 × 11	10.95 ± 0.15
CINy02.103	30	10.37 ± 0.15
CINy03.105	25	14.72 ± 0.17

The photon yield is estimated as the expected number of p.e. for a $Z = 1$, $\beta \sim 1$ particle for fully contained rings.

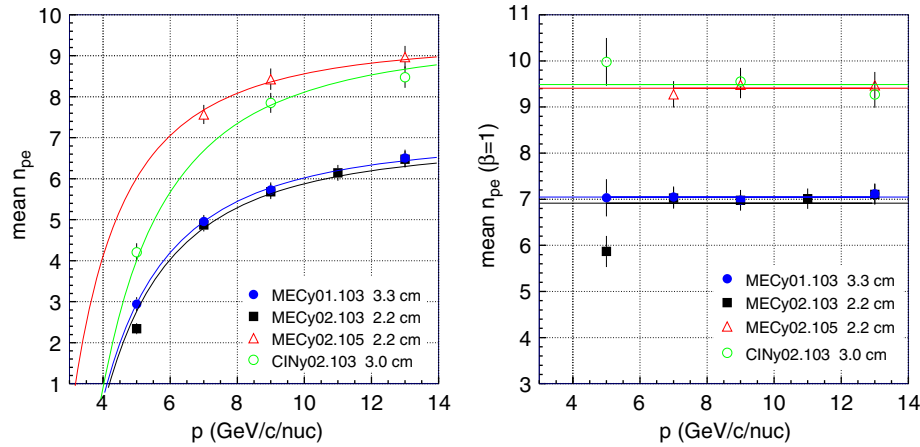


Fig. 6. Mean number of photoelectrons as function of the proton beam momentum for the different tested aerogel radiators (left) and after correcting for the momentum dependence (right).

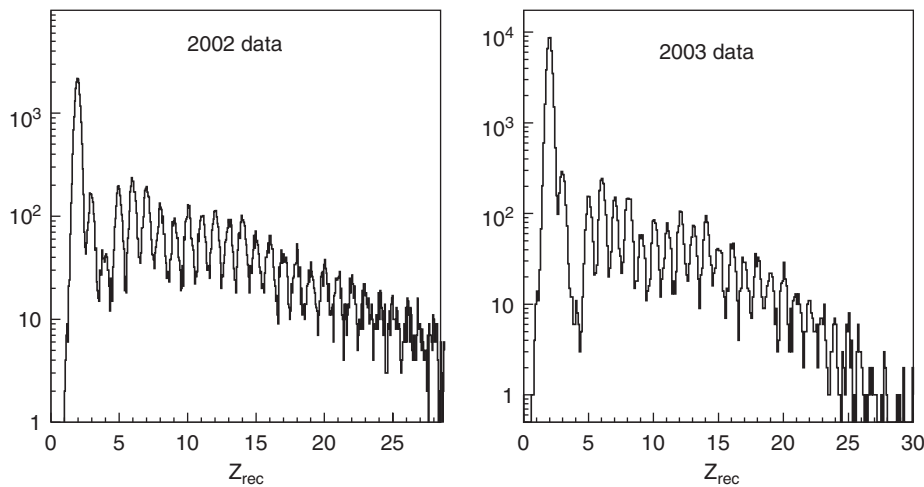


Fig. 7. Reconstructed charge spectra from the measured data, showing the individual elements identification up to $Z \approx 26$ for the CIN aerogel $n = 1.03$ sample, measured with 20 GeV/c/n Pb ion fragments (2002, left), and with 158 GeV/c/n In ion fragments (2003, right), respectively.

The position of the charge peaks follow the expectation up to $Z = 15$. Above this value, a gradual deviation from the linearity reaching a shift of 1 missing charge unit for $Z \sim 30$ is observed. An effective correction for high charge hits ($Q_{\text{hit}} > 26$ p.e.) reduces the non-linearity on the reconstructed charge below 0.1 charge unit in the whole Z range.

The charge resolution for each element was evaluated through individual Gaussian fits to the reconstructed charge distribution on the samples selected by the independent scintillator and silicon detectors (see Fig. 8, left). The results for the CINy02.103 and CINy03.105 are displayed in Fig. 8, right panel, as a function of the charge Z of the particle. The curve corresponds to the error propagation on Z which can be expressed as

$$\sigma(Z) = \frac{1}{2} \left(\frac{1 + \sigma_Q^2}{N_{\text{exp}}} + \left(Z \times \frac{\Delta N_{\text{exp}}}{N_{\text{exp}}} \right)^2 \right)^{1/2} \quad (1)$$

which expresses the charge resolution $\sigma(Z)$ as a function of the photon yield N_{exp} , and of the PMT single p.e. resolution σ_Q , and incorporates a possible contribution arising from the systematics ΔN_{exp} , which is shown to be 1–2%.

As expected, the charge resolution provided by the radiator CINy03.105 is clearly better than that of the CINy02.103, due to its higher photon yield (see Table 2).

5.6. Velocity resolution

The resolution for the β measurement was estimated using a Gaussian fit to the reconstructed β spectrum, as shown in Fig. 9, left panel, for helium nuclei. The charge dependence of the velocity resolution is shown in Fig. 9 for the aerogel CINy02.103. The observed distribution varies like $1/Z$ as it could be expected from the charge dependence of the photon yield in Cherenkov emission, up to a saturation limit set by the pixel size of the detector.

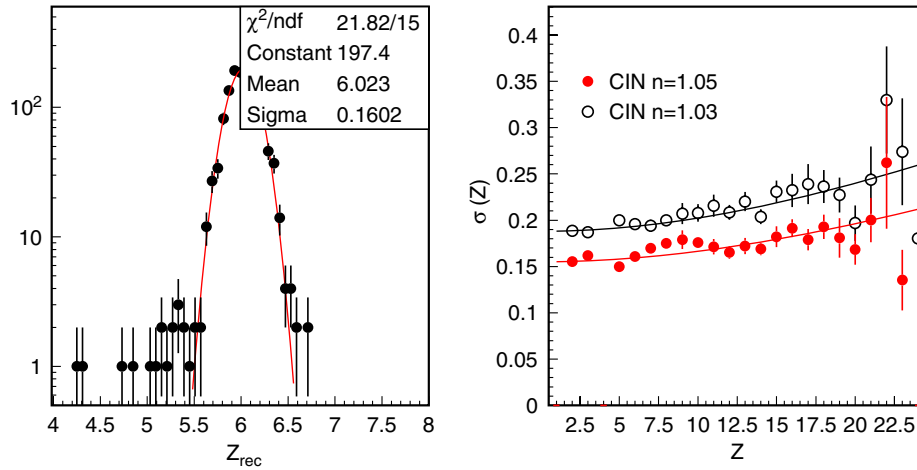


Fig. 8. Left: Charge distribution for a sample of carbon nuclei selected with silicon tracker and scintillators and Gaussian fit. Right: Charge resolution versus particle Z for $n = 1.03$ and $n = 1.05$ CIN aerogel tested in 2003 runs. The curve gives the expected value estimated as explained in the text.

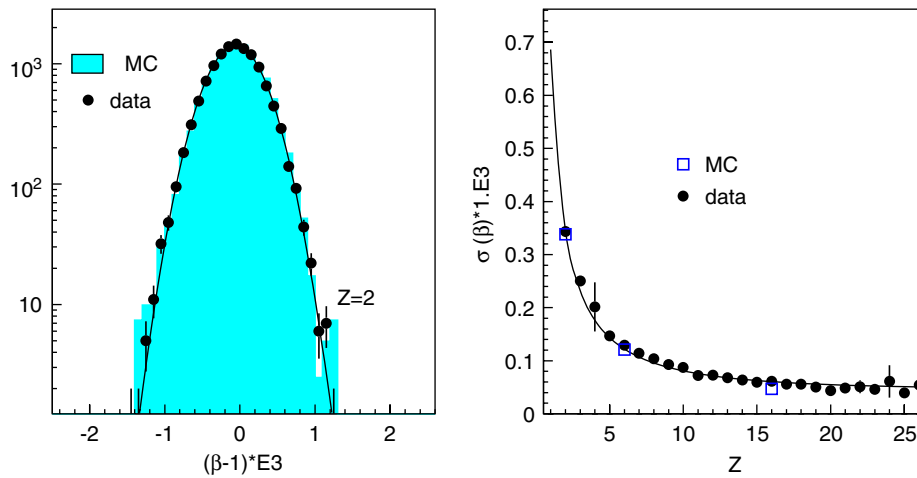


Fig. 9. Left: Velocity distribution for $Z = 2$ particles, data (black points) and MC simulation (grey histogram). A Gaussian fit is applied to data to estimate the resolution. Right: Velocity resolution versus Z for the radiator CINy02.1.03 together with the fitted parametrization described in the text.

The function used to fit the data is the following:

$$\sigma_{\beta}(Z) = \sqrt{\left(\frac{A}{Z}\right)^2 + B^2}. \quad (2)$$

The fitted values of the parameters for the different radiators are in the range $A = 0.7\text{--}1.0 \times 10^{-3}$ and $B = 0.4\text{--}0.6 \times 10^{-4}$.

The values of the measured β resolution are given in Table 3. The data refer to runs with different expansion distances H set in order to have fully contained rings. Due to the dependence of $\sigma(\beta)$ with the expansion distance, a direct comparison of the performances for different radiators should be done on the basis of runs with same distance (rightmost column). For the 2002 run this value has been extrapolated by means of the MC simulation. The best resolution is obtained with the $n = 1.03$ CIN sample, even compared with the same refractive index and smaller thickness MEC sample.

Table 3

Velocity resolution $\sigma(\beta)/\beta$ in 10^{-3} units obtained for protons ($Z = 1$) and ^4He particles ($Z = 2$) for the studied radiators with different expansion distances, and, in the rightmost column, with the same distance ($H = 33.45$ cm) in order to have a fair comparison of the radiators

Radiator	H (cm)	$(\sigma_{\beta}/\beta)^{\text{meas}}$		$(\sigma_{\beta}/\beta)_{H=33.4, \beta=1}$
		$Z = 1$	$Z = 2$	$Z = 2$
<i>2002 run</i>				
MECy01.103	42.25	0.67 ± 0.10	0.45 ± 0.03	0.54 ± 0.02 (*)
MECy02.103	42.25	0.63 ± 0.04	0.43 ± 0.03	0.48 ± 0.02 (*)
MECy02.105	37.5	0.95 ± 0.08	0.49 ± 0.03	0.51 ± 0.02 (*)
CINy02.103	42.25	0.65 ± 0.01	0.35 ± 0.02	0.45 ± 0.02 (*)
<i>2003 run</i>				
MECy03.103	42.3	–	0.364 ± 0.001	0.49 ± 0.03
CINy02.103	42.3	–	0.343 ± 0.001	0.45 ± 0.01
CINy03.105	35.3	–	0.443 ± 0.002	0.48 ± 0.02

Values labelled with the asterisk are an extrapolation based on MC simulation.

5.7. Radiator modelling

A Monte Carlo simulation of the prototype has been developed in order to quantify the difference between the tested radiators. The simulation parameters used here were:

- The refractive index, adjusted to reproduce the mean β value of the beam particles.
- The Rayleigh scattering length L_R , parametrized using the clarity coefficient C as $L_R = \lambda^4/C$. The value of C was adjusted to match the photon yield of the data.
- The absorption length, measured using a photo-spectrometer for a single tile [25–27]. The obtained value is one order of magnitude larger than the mean photon path length inside the radiators. Absorption is therefore negligible compared to Rayleigh scattering.

The beam profile, rigidity spread, and angular divergence have been simulated according to their experimental values to evaluate the expected velocity resolution for each run. The comparison of the resolution measured on helium particles and the corresponding simulation shows a disagreement ranging from 20% up to more than 50% depending on the radiator sample. The large variations of the observed differences among radiators with the same refractive index and geometry discard the beam features as the source of the disagreement. For the same reason, the cross-talk in the PMT light guides or inside the photomultipliers are also ruled out as the main origin of the observed difference. The aerogel properties are left as the most likely origin of the disagreement.

5.7.1. Forward photon scattering

Since absorption and Rayleigh scattering fail to fully account for the Cherenkov yield in the studied samples with a good enough accuracy and since the simulation results underestimate the experimental values of $\sigma(\beta)$, another source of photon dispersion has to be considered. The missing dispersion source is most likely to originate from the forward scattering (FS) effect. This surface effect was first observed and studied in Ref. [28], and recently thoroughly investigated in Ref. [29] in the context of the RICH detector instrumentation.

In the present case, the effect has been taken into account as follows. Each photon refracted out of the radiator was assigned a probability P_{col} of scattering on a surface cluster. In this case, the photon is forward scattered, with an angular distribution described by the functional form: $P(\theta) = (\sin \theta / \delta \theta^2) \exp(-\sin^2 \theta / 2\delta \theta^2)$.

This implies that part of the photons on the prototype are scattered away from the reconstructed ring, and previous determination of C suffered a large systematic error due to this photon loss. A new determination of the clarity coefficient C taking into account this effect is necessary to complete the model. The model parameters, except for C , were determined by adjusting the distribution of the β residue for each hit. The results are illustrated in

Fig. 10. The two parameter fits ($P_{\text{col}}, \delta \theta$) allow to obtain an agreement with the data at the percent level.

The values of the $P_{\text{col}}, \delta \theta$, and C parameters, together with the corresponding values of the ratio $[\sigma(\beta)]_{\text{data}} / [\sigma(\beta)]_{\text{simulation}}$ obtained in the analysis, are given in Table 4. The agreement between simulation and data is seen to be better than 5% for all the studied radiators but the MECy01.103, which is at the 10% level. Note that the values of C correspond to an effective clarity coefficient because they are strongly correlated in the analysis with other parameters not tightly controlled such as the quantum efficiency of the PMT photocathodes.

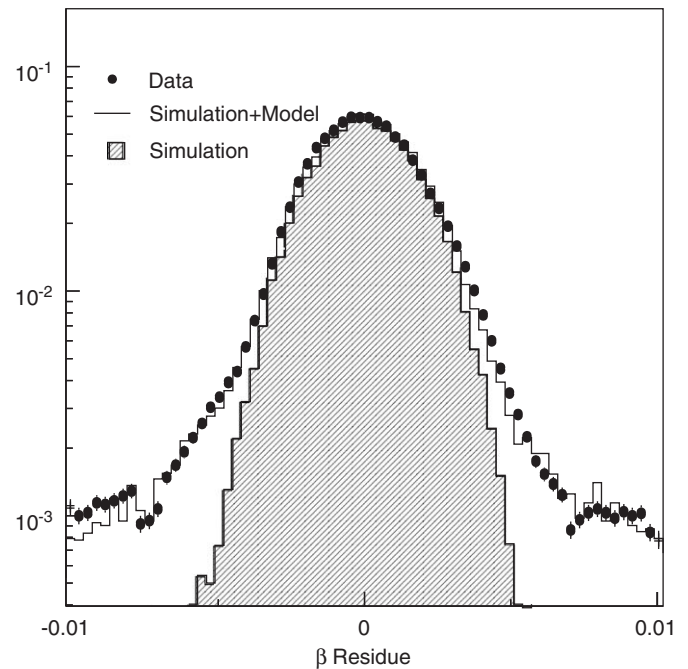


Fig. 10. Distribution of the β residues for the data, the simulation, and the simulation plus the forward scattering component.

Table 4

Values of the $P_{\text{col}}, \delta \theta$, and C parameters characterizing the optical properties of the aerogel material as defined in the text, and values of the ratio of the measured to the simulated velocity resolutions $R = [\sigma(\beta)]_{\text{data}} / [\sigma(\beta)]_{\text{simu}}$, obtained in the analysis, for the studied samples

Radiator	P_{col}	$\delta \theta$ (mrad)	C ($\mu\text{m}^4 \text{cm}^{-1}$)	R
<i>2002 run</i>				
MECy01.103	0.33 ± 0.02	20 ± 3	0.0089 ± 0.0002	1.13 ± 0.01
MECy02.103	0.28 ± 0.02	24 ± 2	0.0079 ± 0.0001	0.96 ± 0.01
MECy02.105	0.20 ± 0.02	25 ± 3	0.0095 ± 0.0002	0.96 ± 0.01
CINy02.103	0.15 ± 0.01	24 ± 3	0.0059 ± 0.0001	0.98 ± 0.01
<i>2003 run</i>				
MECy03.103	0.14 ± 0.01	23 ± 2	0.0058 ± 0.0001	0.98 ± 0.01
CINy02.103	0.14 ± 0.01	17 ± 2	0.0052 ± 0.0001	1.03 ± 0.01
CINy03.105	0.19 ± 0.01	14 ± 2	0.0055 ± 0.0001	1.00 ± 0.02

The associated error accounts for the systematics of the radiator modelling method.

Nevertheless, the fair agreement with the values obtained from direct measurements [26] gives confidence to the results of the analysis.

The discrepancy observed in the fitted $\delta\theta$ values of the radiator CIny02.103 between the 2002 and 2003 runs is due to the different beam conditions for the two runs (see Section 4.1).

6. Discussion of the results

One purpose of the study was to select a Cherenkov radiator with the best optical properties within the considered range of refraction index, and matching some other requirements related to the chemical, physical, geometrical or mechanical properties of the material, set by the counter design and operation conditions.

In Table 3, clearly three samples emerge from the studied set with the best performances: CIny02.103, MECy03.103, CIny03.105. A first option has to be taken with respect to the larger and lower index value to be used. Using an $n = 1.05$ Cherenkov radiator ensures a larger photon yield and thus a better charge separation, to the price of a slightly poorer velocity resolution. This is particularly safe for $Z = 1$ particles for which the light production would keep the reconstruction efficiency at a good level through time. It is a more robust option than $n = 1.03$ and has been taken for this reason in the prospect of the three-year mission on the ISS. This option points the CIny03.105 material as the best candidate.

Two further considerations have to be mentioned: (a) The MEC products are available only in 1 cm thick tiles, and stacking several tiles would increase the possible surface scattering of photons, although no such significant effect has been observed in the study. (b) The CIN aerogel is hygrophylic and it would suffer with degradation of its optical properties in a humid environment (with physical damages for very humid atmosphere), while the MEC material is hydrophobic and thus easier to use. However, keeping the radiator plane in a dry environment in the AMS spectrometer is easily achievable and does not raise any major technical difficulty. A possible deterioration on long-term period of the hygrophylic aerogel has been excluded by the comparison of the performance of a CIN sample in the 2002 and 2003 runs: after one year of shelf storage this aerogel did not show any apparent loss of transparency (see Section 5.4).

All these considerations lead to the final choice of the Novosibirsk $n = 1.05$ aerogel (CIny03.105).

Nevertheless, in order to ensure its resistance to the environment conditions on the ISS a series of tests to measure the mechanical and optical properties in the laboratory have been made. Several measurements of transmittance, resistance to thermal cycles and mechanical vibration have been performed and up to now no unexpected deterioration has been observed. A future publication will report on the results of these tests [26].

7. Summary and conclusion

In summary, a prototype of the AMS imager in a version close to the flight model has been built and thoroughly studied. The response and the transmission properties of the photosensitive and of the optical components of the detector have been tested over the expected range of sensitivity (visible range of the Cherenkov spectrum) and the apparatus has been calibrated. An end-to-end test of the instrument has been performed with cosmic muons on the ground and with a beam ion distribution close to the natural cosmic ray abundance.

The tests have allowed to validate the FE electronics. Excellent data have been collected on the response of the detector to ions over the range $1 \leq Z < 30$, which made possible to achieve accurate measurements of the velocity ($\sigma(\beta)/\beta$ better than 10^{-3} for $Z = 1$ particles) and charge resolutions ($\sigma(Z)/Z \approx 0.2$) of the counter through the range of nuclear species required by the scientific program of the collaboration. The results are in fair agreement with the expectations. The final detector should thus match the requirements of an ambitious program of measurements of the cosmic ray flux with a high-efficiency apparatus and high counting statistics collected.

The study has included a fruitful in-depth study of the aerogel radiators properties. In particular, it has been shown that the surface scattering contribution has to be included in the data analysis for the results to be accurately accounted for, and a sound determination of the optical parameters of the studied radiator samples has been obtained. The results of this work have provided the basis on which the final choice of the aerogel radiator to equip the flight model of the detector could be made.

Finally, it has been shown that the design of the RICH counter of the AMS experiment is now completed. The instrumental and technical solutions have been successfully tested over two generations of prototypes. The construction of the flight model of the detector has started at the beginning of 2005 and is now under way.

Acknowledgements

The authors are grateful to the SPS CERN staff for providing the SPS ion beam, and particularly to I. Efthymiopoulos for his constant availability and for his fruitful work in the secondary beam tuning. They are also grateful to the Budker Institute from Novosibirsk (A. Danilyuk, E. Kravchenko, and A. Onuchin), and to the Hamamatsu Company, for providing aerogel tests samples, to J. Berger (LPSC) for his help in the CERN run preparation, to Y. Yoshizawa (Hamamatsu Inc.) for technical informations provided to the authors, and to I. Pshenichnov for making his ion fragmentation cross-section calculations available to the authors for the secondary beam study. A. Menchaca-Rocha and E. Belmont acknowledge support of DGAPA-UNAM Project IN101501, and CONACYT Projects G39091-E and

44380-F. A. Barrau, M. Buénerd, L. Derome and K. Protasov acknowledge partial support from the INTAS Program 03-52-5579.

References

- [1] The AMS Collaboration, *Phys. Rep.* 366 (2002) 331.
- [2] J. Alcaraz, et al., *Nucl. Instr. and Meth. A* 78 (2002) 119.
- [3] J. Séguinot, T. Ypsilantis, *Nucl. Instr. and Meth. A* 343 (1994) 30.
- [4] D.E. Fields, et al., *Nucl. Instr. and Meth. A* 349 (1994) 431.
- [5] T. Thuillier, et al., *Nucl. Instr. and Meth. A* 491 (2002) 83.
- [6] M. Buénerd, Z. Ren, *Nucl. Instr. and Meth.* 454 (2000) 476.
- [7] M. Buénerd, I. Efthymiopoulos, Report CERN-AB-2003-052, May 2003.
- [8] M. Buénerd, *Nucl. Instr. and Meth. A* 502 (2003) 158.
- [9] A. Bouchet, et al., *Nucl. Phys. A* 688 (2001) 417c.
- [10] J. Casaus, et al., Proceedings of 28th International Cosmic Ray Conference (ICRC 2003), July 31–August 7, 2003, Tsukuba, Japan.
- [11] M. Buénerd, AMS internal note 2000-05-06; L. Arruda, Master Thesis, Universidade Técnica de Lisboa, 2003; AMS Internal Report 2004-03-05.
- [12] E. Lanciotti, Master Thesis, Universidad Complutense de Madrid, June 30, 2003.
- [13] Hamamatsu Photonics (<http://www.hamamatsu.com>).
- [14] L. Gallin-Martel, et al., *Nucl. Instr. and Meth. A* 504 (2003) 273; L. Gallin-Martel, J. Pouxe, O. Rossetto, M. Yamoumi, Proceedings of 2001 IEEE Nuclear Science Symposium, November 4–10, 2001, San Diego, California.
- [15] G. Castellini (guido@ALPHA1.iroecfi.cnr.it), private communication.
- [16] J. Marin, et al., *Informes Técnicos CIEMAT* 1011 (2002) ISSN 1135-9420.
- [17] G. Boudoul, Thèse, Université J. Fourier Grenoble, France, September 30, 2003.
- [18] C. Delgado, Thesis, Universidad Autónoma de Madrid, September 15, 2003.
- [19] Y. Yoshizawa, Hamamatsu photonics, private communication
- [20] J. Borges, Master Thesis, Universidade Técnica de Lisboa, 2004; AMS Internal Report 2004-03-06.
- [21] M. Pohl, et al., *Nucl. Phys. B* 122 (223) (Proc. Suppl.) 151.
- [22] Matsushita Electric Works, Ltd., 1048 Kadoma, Osaka 571-8686, Japan.
- [23] Budker Institute of Nuclear Physics, Novosibirsk 630090, Russia, E. Kravtchenko; Borekov Institute of Catalysis Pr. Akademika Lavrentieva, 5 Novosibirsk, Russia, 630090, AF. Danilyuk.
- [24] F. Barao, et al., *Nucl. Instr. and Meth. A* 502 (2003) 310.
- [25] A.F. Danilyuk, et al., *Nucl. Instr. and Meth. A* 494 (2002) 491.
- [26] J. Casaus, et al., in preparation.
- [27] M.F. Villoro, et al., *Nucl. Instr. and Meth. A* 480 (2002) 456.
- [28] P. Wang, et al., *J. Non-Cryst. Solids* (145) (1992) 141.
- [29] R. De Leo, et al., *Nucl. Instr. and Meth. A* 457 (2001) 52.
- [30] M. Aguilar, et al., CIEMAT/2005-1058.